Inorg. Chem. **2008**, *47*, 1165–1172

Synthesis, Characterization, and Reactivity of Iron Trisamidoamine Complexes That Undergo Both Metal- and Ligand-Centered Oxidative Transformations

Remle Çelenligil-Çetin,[‡] Patrina Paraskevopoulou,[†] Rupam Dinda,[†] Richard J. Staples,[§] Ekkehard Sinn,[†] Nigam P. Rath,[#] and Pericles Stavropoulos*,[†]

Department of Chemistry, University of Missouri—Rolla, Rolla, Missouri 65409, Department of Chemistry, Boston University, Boston, Massachusetts 02215, Department of Chemistry and Chemical Biology, Harvard University, Cambridge, Massachusetts 02138, and Department of Chemistry and Biochemistry, University of Missouri—St. Louis, St. Louis, Missouri 63121

Received November 1, 2007

Functional systems that combine redox-active metals and noninnocent ligands are no longer rare chemical oddities; they are instead emerging as significant components of catalytic and enzymatic reactions. The present work examines the synthetic and functional aspects of iron compounds ligated by a family of new trisamidoamine ligands of the type $[(RNC_6H_4)_3N]^{3-}$ (L^1). When R is the electron-rich 4-*t*-Bu–Ph moiety, the ligand can undergo oxidative rearrangement and store oxidizing equivalents under specific conditions. Starting ferrous complexes of the general formula $[(L^1)Fe^{II}solv]^-$ (solv = CH_3CN, dimethylformamide) can be easily oxidized (a) by dioxygen to afford the corresponding $[(L^1)Fe^{III}OH]^-$ complexes, featuring several cases of terminal hydroxo units, and (b) by organochlorides (R–Cl) to provide $[(L^1)Fe^{III}solv]$ congeners and coupled R–R products. Efforts to synthesize $[(L^1)Fe^{III}–O–Fe^{III}(L^1)]^{2-}$ by using $[Cl_3Fe^{III}–O–Fe^{III}Cl_3]^{2-}$ indicate that intrinsic $Fe^{III}Cl$ units can oxidatively rearrange the ligand to afford $[(L^1_{re})(Cl)Fe^{II}][Et_4N]_2$, although the oxidizing equivalent is not retained. Compound $[(L^1_{re})(Cl)Fe^{II}][Et_4N]_2$ can be further oxidized to $[(L^1_{re-2})(Cl)Fe^{III}][Et_4N]$ by CH_2Cl_2. Finally, oxidation of $[(L^1)Fe^{III}solv]$ by $FeCl_3$ affords $[(L^1_{re}H)(Cl)Fe^{II}(\mu\text{-}Cl)_2Fe^{II}(Cl)(L^1_{re-2}H)]$, which features a similar ligand rearrangement that also gives rise to a diamagnetic, doubly oxidized moiety. These results underscore the complexity of chemical transformations available to systems in which both the metal and the ligand are redox-active entities.

Introduction

Metal-bound residues and ligands not only confer necessary structural elements and stereoelectronic properties that can tune the reactivity at the metal site but also may participate in tandem with the metal center to bring about critical chemical and biochemical transformations. Redox-based catalysis, in which both the metal and ligand can possess multiple electronic states during turnover, constitutes a most interesting case of synergistic activity, with a plethora of rapidly accumulating examples of biological importance.[1] Indeed, the growing field of radical enzymology[2] has witnessed a surge of well-defined enzymes (for instance, ribonucleotide reductase,[3] cytochrome *c* peroxidase,[4] galactose oxidase,[5] prostaglandin H synthase,[6] lipoyl synthase,[7] biotin synthase,[8] diol dehydrase,[9] pyruvate formate lyase,[10] DNA photolyase,[11] lysine-2,3-aminomutase[12]) in which met-

* To whom correspondence should be addressed. E-mail: pericles@mst.edu.
[†] University of Missouri—Rolla.
[‡] Boston University.
[§] Harvard University.
[#] University of Missouri—St. Louis.

(1) Stubbe, J.; van der Donk, W. A. *Chem. Rev.* **1998**, *98*, 705–762.
(2) See contributions to the thematic issue: *Chem. Rev.* **2003**, *103*, 2081–2456.
(3) Licht, S.; Gerfen, G. J.; Stubbe, J. *Science* **1996**, *271*, 477–481.
(4) Huyett, J. E.; Doan, P. E.; Gurbiel, R.; Houseman, A. L. P.; Sivaraja, M.; Goodin, D. B.; Hoffman, B. M. *J. Am. Chem. Soc.* **1995**, *117*, 9033–9041.
(5) Whittaker, J. W. *Arc. Biochem. Biophys.* **2005**, *433*, 227–239.
(6) Dorlet, P.; Seibold, S. A.; Babcock, G. T.; Gerfen, G. J.; Smith, W. L.; Tsai, A. L.; Un, S. *Biochemistry* **2002**, *41*, 6107–6114.
(7) Cicchillo, R. M.; Iwig, D. F.; Jones, A. D.; Nesbitt, N. M.; Baleanu-Gogonea, C.; Souder, M. G.; Tu, L.; Booker, S. J. *Biochemistry* **2004**, *43*, 6378–6386.
(8) Berkovitch, F.; Nicolet, Y.; Wan, J. T.; Jarrett, J. T.; Drennan, C. L. *Science* **2004**, *303*, 76–79.
(9) Magnusson, O. T.; Frey, P. A. *Biochemistry* **2002**, *41*, 1695–1702.
(10) Knappe, J.; Wagner, A. F. V. *Adv. Prot. Chem.* **2001**, *58*, 277–315.

10.1021/ic702154z CCC: $40.75
Published on Web 01/08/2008

Chart 1

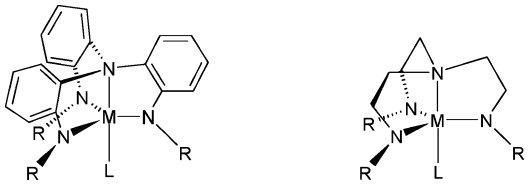

alloradicals, composed of redox-active metals and radical-bearing residues (Tyr•, Cys•, Gly•, Trp•, and $TrpH^{\bullet+}$), operate flawlessly toward storing and transferring redox equivalents, as well as executing mechanistically diverse chemistry (for instance, hydrogen-atom abstraction, proton transfer, single-electron transfer) that is essential for catalytic turnover.[1,2]

The present study explores one member of a family of tripodal trisamidoamine ligands of the type $[(RNC_6H_4)_3N]^{3-}$ (Chart 1, left), recently synthesized by a generic methodology. Under certain oxidative conditions, iron complexes of this ligand, where R is an electron-rich aryl group (R = 4-*t*-Bu−Ph in this study), can generate ligand-centered radicals, which, in turn, are responsible for rearranging the ligand and storing oxidation equivalents in certain cases. Unlike the exhaustively explored $[(RNCH_2CH_2)_3N]^{3-}$ (TREN) systems (Chart 1, right),[13] this noninnocent ligand system also features a more rigid backbone than TREN does and a lack of α-hydrogen atoms with respect to nitrogen residues (β vs the metal), which can be vulnerable in oxidative environments. These stability rules have been highlighted in Collins' development of oxidatively stable tetraamido macrocyclic ligands.[14] Typical β-hydride eliminations from the backbone of the TREN ligand have also been reported,[15] leading to the loss of an arm via C−N(amine) bond cleavage. TREN-type systems have been otherwise superbly exploited in molybdenum/tungsten-based dinitrogen reductive chemistry[16] and in some early-transition-metal organometallic chemistry.[17] More closely to the theme of this work, TREN-type ligands supported an $Fe^{IV}CN$ moiety[18] and gave rise to some unique terminal $Fe^{III}O$ and $Fe^{II/III}OH$ units.[19]

While the short-term goal of the present work is to explore the fundamental chemistry of the new family of ligands under redox conditions, it is the long-term intention of this research to provide conditions that would enable simultaneous support of both high-valent metal−oxo moieties and ligand-centered radicals in mediation of oxygenation chemistry. A summary of the crystallographic data collected in this work is presented in Table 1.

Results and Discussion

Ligand Synthesis and Characterization. Ligand L^1H_3 has been synthesized according to the general three-step methodology depicted in Scheme 1. The tripodal 2,2′,2″-trinitrotriphenylamine is first synthesized by prolonged heating of an 1:3 mixture of 2-nitroaniline and 2-fluoronitrobenzene in dimethyl sulfoxide (DMSO), following modification of a previously published procedure.[20] The product is obtained in 50% yield along with the bipodal 2,2′-dinitrodiphenylamine, which is removed via washings with hot acetone. A previously reported methodology[20] gave large amounts of the bipodal byproduct, whereas attempted Ullmann-type coupling, by heating a neat solution of 2-fluoronitrobenzene over copper powder at 180 °C, resulted in only miniscule amounts of the desired product.

The tripodal trinitroamine is then reduced to the corresponding 2,2′,2″-triaminotriphenylamine by means of pressurized dihydrogen over palladium/carbon in ethanol at 60 °C. The product can be separated from palladium by dissolving it in hot acetone under an inert atmosphere. Small amounts of nitro precursors can be removed by washing the product with hot hexane. The product can be further purified by column chromatography on silica gel (3:1 petroleum ether/ethyl acetate). The structure of this new precursor compound, recrystallized from benzene, is shown in Figure S1 in the Supporting Information.

The synthesis concludes with the $Pd_2(dba)_3$/BINAP-catalyzed coupling of 2,2′,2″-triaminotriphenylamine with 4-*tert*-butylbromobenzene, following standard Hartwig−Buchwald methodology[21] for the arylation of amines. The product is obtained as an off-white solid after purification by column chromatography on silica gel (hexane/ethyl acetate). Recrystallization from hexane affords a good-quality crystalline material suitable for X-ray analysis.

The structure of L^1H_3 (Figure S2 in the Supporting Information) reveals a preorganized cavity (pseudo-C_3-symmetric) that is suitable for tetradentate metalation. Benchmark metrical parameters, which will be used to evaluate ligand rearrangements noted in subsequent sections, include the average C−C distance of the phenyl rings in the triphenylamine core (1.387 Å), with values ranging between 1.371(5) to 1.407(5) Å, and the average C−N(secondary) bond length at 1.402(4) Å.

Synthesis and Characterization of Starting Iron(II) Complexes. Entry into the chemistry of the metalated ligand L^1H_3 is best accomplished by first synthesizing ferrous precursor species. The ligand is deprotonated with 3 equiv

(11) Cheek, J.; Broderick, J. B. *J. Am. Chem. Soc.* **2002**, *124*, 2860−2861.
(12) Banerjee, R. *Chem. Rev.* **2003**, *103*, 2083−2094.
(13) (a) Schrock, R. R. *Acc. Chem. Res.* **1997**, *30*, 9−16. (b) Verkade, J. G. *Acc. Chem. Res.* **1993**, *26*, 483−489.
(14) (a) Collins, T. J. *Acc. Chem. Res.* **1994**, *27*, 279−285. (b) Bartos, M. J.; Gordon-Wylie, S. W.; Fox, B. G.; Wright, L. J.; Weintraub, S. T.; Kauffmann, K. E.; Münck, E.; Kostka, K. L.; Uffelman, E. S.; Rickard, C. E. F.; Noon, K. R.; Collins, T. J. *Coord. Chem. Rev.* **1998**, *174*, 361−390.
(15) Freundlich, J. S.; Schrock, R. R.; Davis, W. M. *J. Am. Chem. Soc.* **1996**, *118*, 3643−3655.
(16) (a) Yandulov, D. V.; Schrock, R. R. *Science* **2003**, *301*, 76−78. (b) Yandulov, D. V.; Schrock, R. R. *J. Am. Chem. Soc.* **2002**, *124*, 6252−6253. (c) Greco, G. E.; Schrock, R. R. *Inorg. Chem.* **2001**, *40*, 3850−3860. (d) Greco, G. E.; Schrock, R. R. *Inorg. Chem.* **2001**, *40*, 3861−3878.
(17) (a) Schrock, R. R.; Adamchuk, J.; Ruhland, K.; Lopez, L. P. H. *Organometallics* **2003**, *22*, 5079−5091. (b) Kim, Y.; Verkade, J. G. *Organometallics* **2002**, *21*, 2395−2399.
(18) Cummins, C. C.; Schrock, R. R. *Inorg. Chem.* **1994**, *33*, 395−396.
(19) (a) Gupta, R.; Borovik, A. S. *J. Am. Chem. Soc.* **2003**, *125*, 13234−13242. (b) MacBeth, C. E.; Golombek, A. P.; Young, V. G., Jr.; Yang, C.; Kuczera, K.; Hendrich, M. P.; Borovik, A. S. *Science* **2000**, *289*, 938−941.
(20) Gorvin, J. H. *J. Chem. Soc., Perkin Trans. 1* **1988**, *6*, 1331−1335.
(21) (a) Hartwig, J. F.; Kawatsura, M.; Hauck, S. I.; Shaughnessy, K. H.; Alcazar-Roman, L. M. *J. Org. Chem.* **1999**, *64*, 5575−5580. (b) Wolfe, J. P.; Buchwald, S. L. *J. Org. Chem.* **2000**, *65*, 1144−1157.

Scheme 1

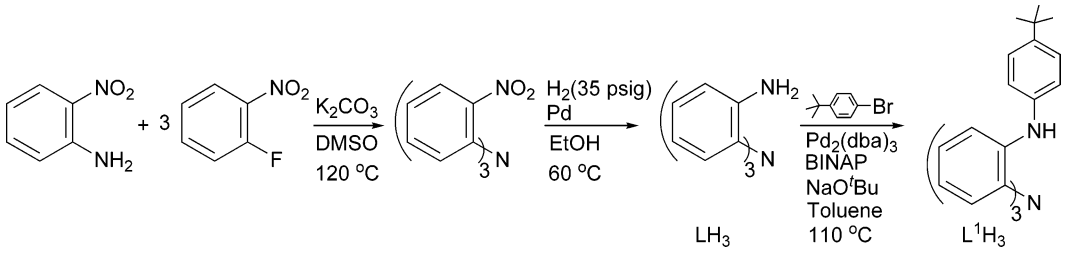

Table 1. Summary of the Crystallographic Data for 2,2′,2″-Triaminotriphenylamine (LH_3), L^1H_3, and **1**−**9**

	LH_3	L^1H_3	**1**	**2**	**3**
formula	$C_{21}H_{21}N_4$	$C_{48}H_{54}N_4$	$C_{80}H_{83}FeN_8P$	$C_{76}H_{80}FeN_5O_{1.5}P$	$C_{114}H_{158}Fe_2K_2N_{14}O_{14}$
M_r	329.42	686.95	1243.36	1174.27	2138.44
cryst syst	monoclinic	monoclinic	monoclinic	monoclinic	cubic
space group	$P2_1/c$	$P2_1/n$	$P2_1/n$	$P2_1/n$	$Pa\bar{3}$
a (Å)	7.9816(4)	16.452(2)	10.6554(17)	10.579(2)	22.3171(6)
b (Å)	14.0735(7)	13.4243(19)	23.765(4)	24.040(5)	22.3171(6)
c (Å)	15.3216(8)	19.063(3)	28.125(6)	28.361(6)	22.3171(6)
α (deg)	90	90	90	90	90
β (deg)	97.4100(10)	107.673(3)	98.872(8)	98.580(6)	90
γ (deg)	90	90	90	90	90
V (Å^3)	1706.69(15)	4011.5(10)	7037(2)	7132(3)	11115.1(5)
Z	4	4	4	4	4
D_{calcd} (g/cm^3)	1.282	1.137	1.174	1.094	1.278
T (K)	173(2)	213(2)	293(2)	293(2)	100(2)
λ (Å)	0.710 73	0.710 73	0.710 73	0710 73	0.710 73
μ (mm^{-1})	0.078	0.066	0.286	0.279	0.404
R1[a] (4σ data)	0.0400	0.0738	0.0824	0.0792	0.1253
wR2[b] (4σ data)	0.0864	0.2050	0.2135	0.1918	0.3323

	4	**5**	**6**	**7**	**8**	**9**
formula	$C_{57}H_{79}FeN_4O_8$	$C_{51}H_{58}FeN_5O$	$C_{50}H_{54}FeN_5$	$C_{68}H_{101}ClFeN_5O$	$C_{60}H_{81}ClFeN_5O$	$C_{99}H_{111}Cl_4Fe_2N_8$
M_r	1004.09	812.87	780.83	1108.35	979.60	1666.46
cryst syst	orthorhombic	rhombohedral	rhombohedral	monoclinic	orthorhombic	triclinic
space group	*Pbca*	$R\bar{3}$	$R\bar{3}$	$P2_1/n$	$P2_12_12_1$	$P\bar{1}$
a (Å)	22.520(10)	14.741(15)	14.710(3)	10.804(6)	10.483(4)	10.4415(14)
b (Å)	22.520(13)	14.741(15)	14.710(3)	31.363(18)	17.586(6)	14.8145(18)
c (Å)	22.520(13)	36.61(5)	36.630(9)	20.186(8)	29.606(10)	16.309(2)
α (deg)	90	90	90	90	90	100.006(3)
β (deg)	90	90	90	94.522(13)	90	94.584(3)
γ (deg)	90	120	120	90	90	109.878(3)
V (Å^3)	11422(11)	6890(14)	6865(3)	6819(6)	5458(3)	2309.9(5)
Z	8	6	6	4	4	1
D_{calcd} (g/cm^3)	1.168	1.175	1.133	1.045	1.192	1.198
T (K)	293(2)	293(2)	296(2)	293(2)	100(2)	293(2)
λ (Å)	0.710 73	0.710 73	0.710 73	0.710 73	0.710 73	0.710 73
μ (mm^{-1})	0.318	0.369	0.367	0.300	0.369	0.479
R1[a] (4σ data)	0.0985	0.0862	0.1068	0.0813	0.0575	0.1159
wR2[b] (4σ data)	0.2720	0.2780	0.2358	0.2053	0.0801	0.1808

[a] $R1 = \sum||F_o| - |F_c||/\sum|F_o|$. [b] $wR2 = [\sum w(F_o^2 - F_c^2)^2/\sum w(F_o^2)^2]^{1/2}$.

of KH in tetrahydrofuran (THF) to afford the air-sensitive compound K_3L^1, which precipitates from saturated THF solutions as a light-yellow solid. The reaction of K_3L^1 (generated in situ in THF) with 1 equiv of anhydrous $FeCl_2$, added as a solid to the THF solution of K_3L^1 under strictly anaerobic conditions, affords green-brown solutions of $[(L^1)Fe^{II}THF]^-$, whose characterization and reactivity will be discussed elsewhere. These solutions are oxidatively unstable even under the most stringent conditions. A more manageable iron(II) precursor can be achieved by changing the solvent to CH_3CN and by using a bulky countercation such as Ph_4P^+. The addition of $[Ph_4P]Cl$ to the deep-green-brown solution of $[(L^1)Fe^{II}THF]^-$ in CH_3CN generates an orange-yellow solution, which upon standing affords orange crystals of $[(L^1)Fe^{II}NCCH_3][Ph_4P]$ (**1**). The structure of **1** (Figure 1) reveals a distorted trigonal-bipyramidal geometry around the ferrous site, with metrical parameters [average $Fe-N_{amido}$ 2.027 Å; $Fe-N_{amine}$ 2.247(5) Å; $Fe-N_{CH_3CN}$ 2.126(6) Å] that are typical of iron(II) complexes. The average $N_{amido}-Fe-N_{amine}$ bond angle (79°) signifies the most important deviation from ideal trigonal-bipyramidal geometry, arising because of the constraints imposed by the five-membered metallocycles. The iron atom is found at an approximate distance of 0.375 Å off the plane formed by the three amido nitrogen atoms, in the direction of the fifth coordination site occupied by acetonitrile. The Fe(1)−N(5)−C(49) angle at 153.4(6)° indicates that the coordination of acetonitrile deviates from the usually linear η^1-CH_3CN coordination mode.[22] Space-filling models indicate strain constraints imposed by the interaction of acetonitrile, en-

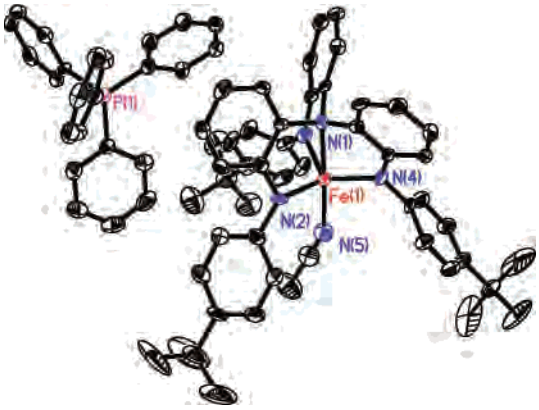

Figure 1. Solid-state structure of **1** showing 50% probability ellipsoids and the atom-labeling scheme. Selected interatomic distances (Å) and angles (deg): Fe(1)−N(4) 2.012(4), Fe(1)−N(3) 2.024(4), Fe(1)−N(2) 2.045(4), Fe(1)−N(5) 2.126(6), Fe(1)−N(1) 2.247(5), N(5)−C(49) 1.125(8); N(4)−Fe(1)−N(3) 119.92(17), N(4)−Fe(1)−N(2) 118.79(16), N(3)−Fe(1)−N(2) 111.20(17), N(4)−Fe(1)−N(5) 102.97(19), N(3)−Fe(1)−N(5) 101.79(19), N(2)−Fe(1)−N(5) 96.99(18), N(4)−Fe(1)−N(1) 78.94(17), N(3)−Fe(1)−N(1) 79.25(16), N(2)−Fe(1)−N(1) 79.82(16), N(5)−Fe(1)−N(1) 176.79(16), C(49)−N(5)−Fe(1) 153.4(6).

capsulated in the cavity of the phenyl arms, along with the bulky *tert*-butyl substituents. It is also noted that the acidic protons of CH_3CN make close contact with the electron-rich, N(2)-atom-appended aryl arm of the ligand (3.104 Å from the center of the phenyl ring), suggesting the possibility of a $\pi_{aryl}-H_{CH_3CN}$ interaction.

Synthesis and Characterization of Ferric Species via Oxidation of Iron(II) Precursors by Dioxygen. (a) Reactions in CH_3CN. Green solutions of $[(L^1)Fe^{II}NCCH_3]^-$ in CH_3CN can be oxidized with dioxygen to afford dark-blue solutions, from which a crystalline material that is not suitable for X-ray analysis can be obtained. Cation exchange with $[PPh_4]Cl$, dissolved in blue acetonitrile solutions of this crystalline material, affords $[(L^1)Fe^{III}OH][PPh_4]\cdot CH_3CN\cdot 0.5Et_2O$ (**2**) upon diffusion of diethyl ether.

The structure of **2** (Figure 2) reveals a terminally coordinating oxygen atom that is assigned to a hydroxide moiety. This is supported by the Fe−OH bond distance at 1.920(4) Å and further established by means of an IR-active $\nu(^{16}O-H)$ band at 3630 cm^{-1}. The average $Fe-N_{amido}$ bond distance at 1.995(5) Å and the significant displacement of the iron atom from the plane of the three amido nitrogen atoms (0.449 Å) are consistent with the presence of a ferric center.

(b) Reactions in Dimethylformamide (DMF). Yellow-green solutions generated from the reaction of K_3L^1 and $FeCl_2$ in DMF, presumably containing the anion $[(L^1)Fe^{II}DMF]^-$, can be oxidized by dioxygen to afford $[(L^1)Fe^{III}OH][K(DMF)_3]\cdot 3H_2O$ (**3**) as dark-blue crystals. The compound has been characterized by X-ray analysis (Figure S3 in the Supporting Information), albeit on poor-quality crystals due to persistent twinning problems. The solid-state structure reveals a terminal hydroxo moiety (Fe−OH = 1.856(11) Å; $\nu(^{16}O-H) = 3615\ cm^{-1}$), whereas the 3-fold $Fe-N_{amido}$ bond distance 1.952(6) Å is typical of a ferric site. The potassium

(22) (a) Barrera, J.; Sabat, M.; Harman, W. D. *Organometallics* **1993**, *12*, 4381−4390. (b) Chetcuti, P. A.; Knobler, C. B.; Hawthorne, M. F. *Organometallics* **1988**, *7*, 650−660.

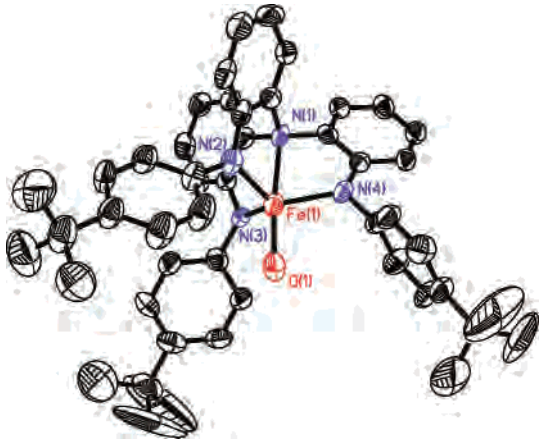

Figure 2. Solid-state structure of **2** showing 50% probability ellipsoids and the atom-labeling scheme. The PPh_4^+ cation is omitted for clarity. Selected interatomic distances (Å) and angles (deg): Fe(1)−O(1) 1.920(4), Fe(1)−N(2) 1.986(5), Fe(1)−N(4) 1.995(5), Fe(1)−N(3) 2.003(5), Fe(1)−N(1) 2.297(5), O(1)−H(1A) 0.8200; O(1)−Fe(1)−N(2) 107.0(2), O(1)−Fe(1)−N(4) 99.5(2), N(2)−Fe(1)−N(4) 118.1(2), O(1)−Fe(1)−N(3) 103.2(2), N(2)−Fe(1)−N(3) 108.0(2), N(4)−Fe(1)−N(3) 118.9(2), O(1)−Fe(1)−N(1) 174.20(18), N(2)−Fe(1)−N(1) 78.1(2), N(4)−Fe(1)−N(1) 75.31(19), N(3)−Fe(1)−N(1) 77.51(19), Fe(1)−O(1)−H(1A) 109.5.

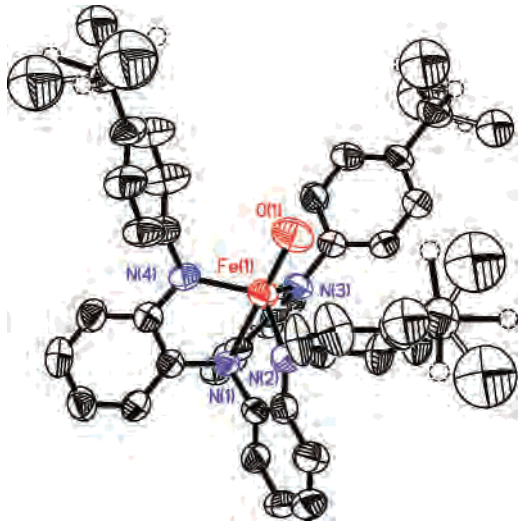

Figure 3. Solid-state structure of **4** showing 50% probability ellipsoids and the atom labeling scheme. Selected interatomic distances (Å) and angles (deg): Fe(1)−O(1) 1.863(5), Fe(1)−N(3) 1.963(6), Fe(1)−N(2) 1.964(6), Fe(1)−N(4) 1.966(6), Fe(1)−N(1) 2.346(5), N(1)−C(13) 1.440(8), N(1)−C(1) 1.445(8), N(1)−C(7) 1.447(8), N(2)−C(2) 1.379(8), N(3)−C(8) 1.375(8), N(4)−C(14) 1.386(8); O(1)−Fe(1)−N(3) 102.1(2), O(1)−Fe(1)−N(2) 102.3(2), N(3)−Fe(1)−N(2) 115.3(2), O(1)−Fe(1)−N(4) 102.3(2), N(3)−Fe(1)−N(4) 115.7(2), N(2)−Fe(1)−N(4) 115.8(2), N(3)−Fe(1)−N(1) 77.9(2), N(2)−Fe(1)−N(1) 77.89(19), N(4)−Fe(1)−N(1) 77.5(2), O(1)−Fe(1)−N(1) 179.7(2).

cation, which is separated from the hydroxo moiety by 5.753 Å, is supported by a matrix of six DMF molecules.

Compound **3** readily absorbs water molecules in the lattice, and, indeed, if the reaction for its preparation is performed with wet dioxygen and/or in wet DMF, then the product obtained is instead crystalline $[(L^1)Fe^{III}OH](H_3O)\cdot 4H_2O$ (**4**). An alternative formulation of the same compound is $[(L^1)Fe^{III}-OH_2]\cdot 5H_2O$, but the former assignment is supported by an Fe−OH bond distance of 1.863(5) Å in **4** (Figure 3) and a $\nu(^{16}O-H)$ vibration at 3616 cm^{-1}, which are very similar to those in **3** and inconsistent with the presence of a coordinated water molecule. The average $Fe-N_{amido}$ and apical $Fe-N_{amine}$

bond distances of 1.964(6) and 2.346(5) Å, respectively, are also very similar to those encountered in **3** and are within the range expected for a ferric site. Potassium ion is not detected by atomic absorption and X-ray analysis; that leaves the hydronium ion as the only reasonable option in the charge-balancing role. Hence, one of the lattice water molecules has been modeled as a hydronium ion involved in hydrogen-atom bonding with solvated water molecules.

In summary, the reaction of $[(L^1)Fe^{II}solv]^-$ (solv = CH_3CN, DMF) with dioxygen leads to the formation of $[(L^1)Fe^{III}OH]^-$ ions in all cases examined. Reactions with $^{18}O_2$ indicate that the hydroxo oxygen atom is derived from dioxygen, but the source of the hydrogen atom, whether due to water traces or hydrogen-atom abstraction, is currently unknown.

Synthesis and Characterization of Ferric Species via Oxidation of Iron(II) Precursors by Dichloromethane and Other Chloroorganics. Solutions of $[(L^1)Fe^{II}solv]^-$ (solv = DMF, CH_3CN) can be easily oxidized by a series of R−Cl (in decreasing order of reactivity, R = benzyl, allyl > *t*-Bu, *i*-Pr ≫ *n*-Bu, Ph) according to the equation

$$2[(L^1)Fe^{II}solv](K) + 2R{-}Cl \rightarrow 2[(L^1)Fe^{III}solv] + R{-}R + 2KCl \quad (1)$$

Details about the scope and mechanism of these reductive dechlorination reactions[23] will be presented elsewhere. In the current context, the reaction can be exploited for its synthetic utility because it affords access to the solvated adducts $[(L^1)Fe^{III}solv]$ [solv = DMF (**5**), CH_3CN (**6**)]. Dichloromethane is the most practical reagent; a few drops, or diffusion, of CH_2Cl_2 in yellow-green solutions of $[(L^1)Fe^{II}solv]^-$ in the corresponding solvent readily generates dark-blue solutions of $[(L^1)Fe^{III}solv]$. Two representative examples [solv = DMF (**5**), CH_3CN (**6**)] have been structurally characterized.

Compound **5** (Figure 4) adopts a C_3-symmetric geometry, featuring a unique Fe(1)−N_{amido} bond distance of 1.946(3) Å, which is shorter than that found in iron(II) complex **1** and consistent with those observed for iron(III) compounds **2**−**4**. The central iron atom Fe(1) lies 0.361 Å above the equatorial plane of the three amido nitrogen atoms and away from the apical N(1) nitrogen atom.

From acetonitrile solutions, the corresponding compound **6** (Figure 5) is obtained, which also features a similar C_3-symmetric configuration. As expected for the ferric state, the average Fe−N_{amido} bond distance of 1.964(6) Å in **6** is shorter than that in **1** [2.027(4) Å], as is the Fe−$NCCH_3$ bond distance in **6** [2.053(17) Å] by comparison to that in **1** [2.126(6) Å]. Accordingly, the C−N bond distance of the coordinated CH_3CN in **6** [1.25(3) Å] is longer than the corresponding C−N bond distance in **1** [1.125(8) Å]. In contrast to the bent Fe−N−CCH_3 moiety in **1**, the corresponding angle in **6** is linear because space-filling models

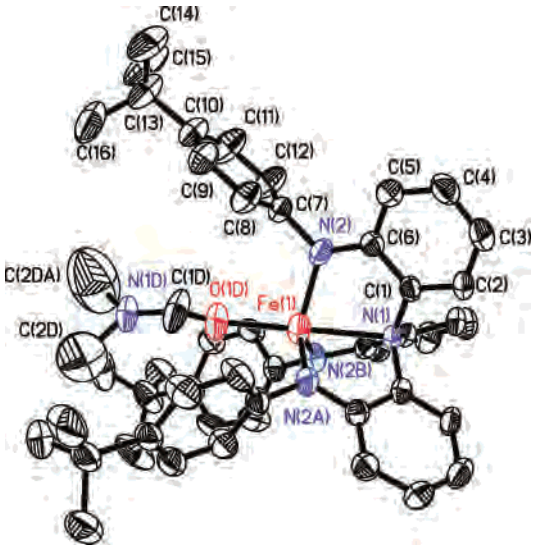

Figure 4. Solid-state structure of **5** showing 50% probability ellipsoids and the atom-labeling scheme. Selected interatomic distances (Å) and angles (deg): Fe(1)−N(2) 1.946(3), Fe(1)−O(1D) 1.980(4), Fe(1)−N(1) 2.230-(4), N(1)−C(1) 1.464(3); N(2A)−Fe(1)−N(2) 116.64(4), N(2)−Fe(1)−O(1D) 100.70(7), O(1D)−Fe(1)−N(1) 180.0, N(2)−Fe(1)−N(1) 79.30(7).

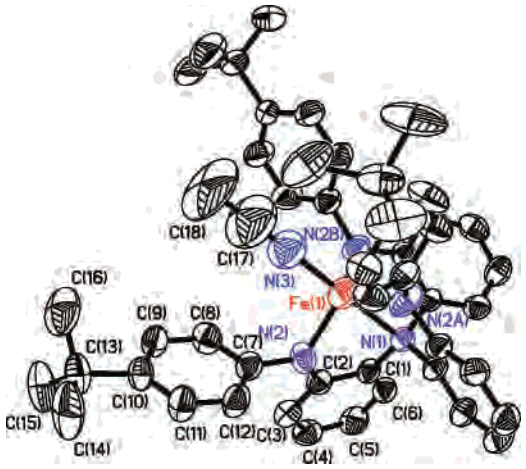

Figure 5. Solid-state structure of **6** showing 50% probability ellipsoids and the atom-labeling scheme. Selected interatomic distances (Å) and angles (deg): Fe(1)−N(2) 1.964(6), Fe(1)−N(3) 2.053(17), Fe(1)−N(1) 2.272-(9), N(3)−C(17) 1.25(3); N(2)−Fe(1)−N(2A) 115.55(13), N(2)−Fe(1)−N(3) 102.36(19), N(2)−Fe(1)−N(1) 77.64(19), N(3)−Fe(1)−N(1) 180.000-(1), C(17)−N(3)−Fe(1) 180.000(2), N(3)−C(17)−C(18) 180.000(3).

indicate that steric interactions with the *t*-Bu groups are reduced in **6**.

Electrochemistry. Cyclic and linear-sweep voltammetry experiments on $[(L^1)Fe^{II}solv]^-$ (solv = DMF, DMSO) under anaerobic conditions are instructive with respect to the oxidative transformations of the iron(II) precursors. In DMF, a semireversible Fe^{II}/Fe^{III} couple is observed at very accessible potentials ($E_{1/2}$ = −1.298 V vs Fc^+/Fc, ΔE = 71 mV, and $i_{p,a}/i_{p,c}$ = 1.16; Figure 6), followed by a two-electron anodic peak at E_a = −0.038 V that is tentatively assigned to simultaneous oxidation of the metal and ligand ($[(L^1)Fe^{II}] \rightarrow [(L^1)^{\bullet}Fe^{III}]$). Similar behavior is observed in DMSO ($E_{1/2}$ = −1.302 V vs Fc^+/Fc, ΔE = 81 mV, and $i_{p,a}/i_{p,c}$ = 1.23; anodic peak at E_a = −0.063 V). Importantly, the corresponding anodic wave in THF is significantly more accessible (E_a = −0.382 V) and as will be detailed elsewhere,

(23) (a) Costentin, C.; Robert, M.; Savéant, J.-M. *J. Am. Chem. Soc.* **2004**, *126*, 16834−16840. (b) Costentin, C.; Robert, M.; Savéant, J.-M. *J. Am. Chem. Soc.* **2003**, *125*, 10729−10739.

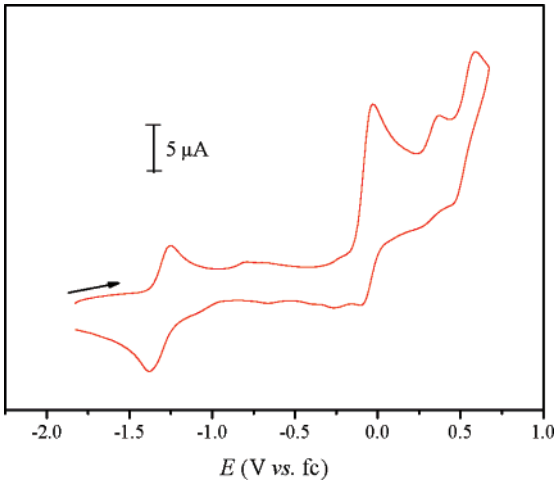

Figure 6. Cyclic voltammetry of $[(L^1)Fe^{II}DMF]^-$ (3 mM) in DMF/0.1 M $TBAPF_6$ with a gold disk electrode (1.6 mm in diameter). Scan rate = 0.1 V/s.

the reaction of $[(L^1)Fe^{II}THF]^-$ with dioxygen in THF leads to both metal- and ligand-centered oxidation. However, ligand-based oxidations are achievable by other strong oxidants, as indicated below.

Incidentally, ligand L^1H_3 and the precursor 2,2′,2″-triaminotriphenylamine, which are stable toward oxygen, exhibit an anodic wave at E_a = 0.325 and 0.295 V, respectively, in DMSO, whereas the deprotonated K_3L^1, which is exceedingly air-sensitive, has the corresponding wave at −0.654 V in DMSO. It is worthwhile mentioning in this context that the oxidation of K_3L^1 with dioxygen (toward so far uncharacterized products) is also associated with a g = 2.0 electron paramagnetic resonance (EPR) signal during the early stages of the reaction, which decays over time. Similar behavior is also observed in the oxidation of $[(L^1)Zn^{II}NCCH_3]^-$, indicating that the ligand does not necessarily require a redox-active metal to undergo oxidation by dioxygen.

Other Oxidizing Agents. (a) In Situ $Fe^{III}Cl$ Moieties. In an effort to synthesize $[(L^1)Fe^{III}-O-Fe^{III}(L^1)]^{2-}$, $[Cl_3Fe^{III}-O-Fe^{III}Cl_3](NEt_4)_2$[24] was added to 2 equiv of K_3L^1 in THF to afford dark-green-black solutions. Rather than obtaining the intended compound, crystals of $[(L^1{}_{re})Fe^{II}Cl](NEt_4)_2$ (**7**) can be isolated from diethyl ether extracts of the reaction mixture upon the addition of hexane. Most importantly, ligand L^1 has been rearranged in **7**, due to formal cleavage of a $N_{amine}-C$ bond and the formation of a new $N_{amido}-C$ bond (Scheme 2). It has been established that this rearrangement is triggered by an initial one-electron oxidation of the ligand at the N_{amido} site, leading to an aminyl radical, which is then involved in an 1,4-(*N*-to-*N*)-phenyl migration, as indicated in Scheme 2. However, the initial oxidizing equivalent is not retained in **7**; hence, $L^1{}_{re}$ remains a trianion.

A second point of importance is that the all-ferric oxidation state of the starting material has been reduced to the ferrous site of compound **7**. Taken together, these observations suggest that $Fe^{III}Cl$ moieties act as internal oxidants of the coordinated ligand, although the oxidizing equivalent is not

(24) Armstrong, W. H.; Lippard, S. J. *Inorg. Chem.* **1985**, *24*, 981−982.

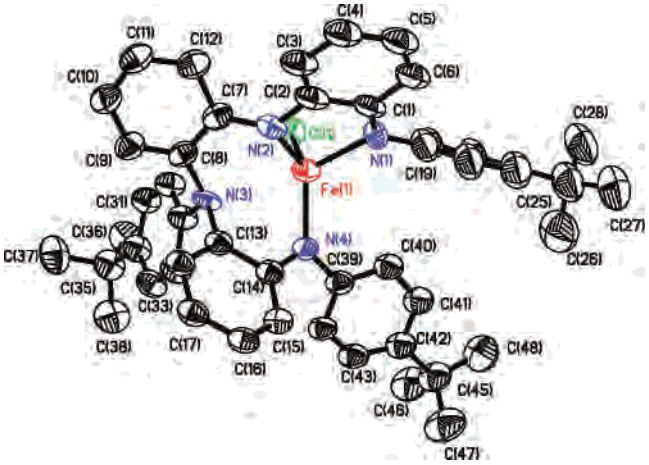

Figure 7. Solid-state structure of **7** showing 50% probability ellipsoids and the atom-labeling scheme ($[Et_4N]$ cations have been omitted for clarity). Selected interatomic distances (Å) and angles (deg): Fe(1)−N(4) 2.019(10), Fe(1)−N(2) 2.090(10), Fe(1)−N(1) 2.106(9), Fe(1)−Cl(1) 2.357(4), Fe(1)−N(3) 2.679(10), N(1)−C(1) 1.316(14), N(1)−C(19) 1.384(16), N(2)−C(7) 1.368(15), N(2)−C(2) 1.417(14), N(3)−C(29) 1.427(14), N(3)−C(8) 1.431(15), N(3)−C(13) 1.444(14), N(4)−C(39) 1.416(14), N(4)−C(14) 1.427(14); N(4)−Fe(1)−N(2) 116.9(4), N(4)−Fe(1)−N(1) 114.1(4), N(2)−Fe(1)−N(1) 81.3(4), N(4)−Fe(1)−Cl(1) 120.1(3), N(2)−Fe(1)−Cl(1) 111.3(3), N(1)−Fe(1)−Cl(1) 106.1(3), N(4)−Fe(1)−N(3) 72.2(3), N(2)−Fe(1)−N(3) 69.0(4), N(1)−Fe(1)−N(3) 148.2(3), Cl(1)−Fe(1)−N(3) 95.5(2).

Scheme 2

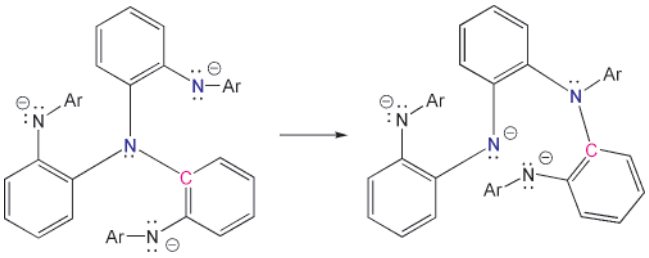

stabilized as a ligand-centered radical within the resulting mononuclear iron(II) compound, and its fate is not known at the present time. The iron(II) state of **7** is supported by the ^{57}Fe Mössbauer effect of **7** at 78 K, which is consistent with the presence of a high-spin ferrous site (δ = 0.99 mm/s, ΔE_Q = 2.84 mm/s, and Γ = 0.44 mm/s), and by the metrical parameters noted below.

As with complexes $[(L^1)Fe^{II}solv]^-$ (solv = DMF, CH_3CN), compound **7** can also be oxidized by dichloromethane to afford the corresponding blue-green ferric complex $[(L^1{}_{re})Fe^{III}Cl](NEt_4)$ (**8**), by allowing CH_2Cl_2 to diffuse into ethereal solutions of **7**.

The structures of **7** (Figure 7) and **8** (Figure 8) are similar and exhibit distorted tetrahedral geometries comprised of the three N_{amido} atoms and the coordinated chloride. The amino nitrogen atom is also found at contact distances of 2.679(10) and 2.501(4) Å from the iron sites of **7** and **8**, respectively, and at a position that caps the facial coordination of the chloride atom and two of the N_{amido} atoms. The average $Fe-N_{amido}$ bond distance in **7** [2.072(10) Å] is significantly longer than that documented in **8** [1.972(5) Å] and comparable to the average $Fe-N_{amido}$ bond distance observed for ferrous species **1**. Similarly, the longer Fe(1)−Cl(1) bond distance [2.357(4) Å] in **7** versus that of **8** [2.301-

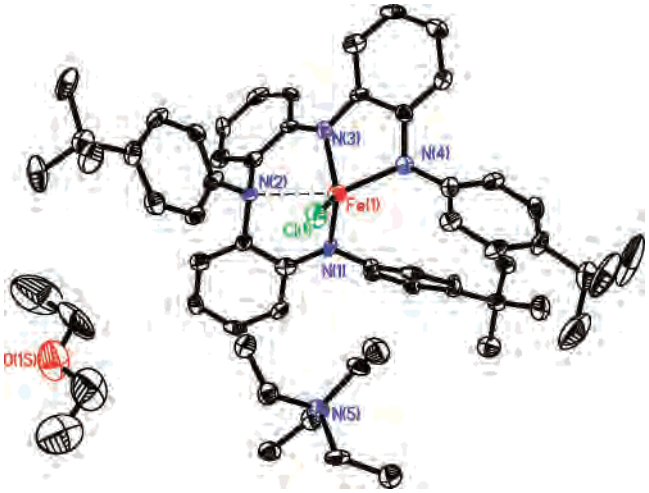

Figure 8. Solid-state structure of **8** showing 50% probability ellipsoids and the atom-labeling scheme. Selected interatomic distances (Å) and angles (deg): Fe(1)−N(3) 1.949(5), Fe(1)−N(1) 1.971(5), Fe(1)−N(4) 1.996(4), Fe(1)−Cl(1) 2.301(2), Fe(1)−N(2) 2.501(4), N(1)−C(1) 1.385(7), N(1)−C(19) 1.434(7), N(2)−C(29) 1.437(7), N(2)−C(2) 1.463(8), N(2)−C(7) 1.466(8), N(3)−C(13) 1.383(6), N(3)−C(8) 1.402(7), N(4)−C(39) 1.407-(6), N(4)−C(14) 1.413(6); N(3)−Fe(1)−N(1) 115.7(2), N(3)−Fe(1)−N(4) 81.59(18), N(1)−Fe(1)−N(4) 117.9(2), N(3)−Fe(1)−Cl(1) 123.38(18), N(1)−Fe(1)−Cl(1) 112.20(16), N(4)−Fe(1)−Cl(1) 101.30(17), N(3)−Fe-(1)−N(2) 74.71(17), N(1)−Fe(1)−N(2) 74.36(19), N(4)−Fe(1)−N(2) 156.29(18), Cl(1)−Fe(1)−N(2) 91.29(14).

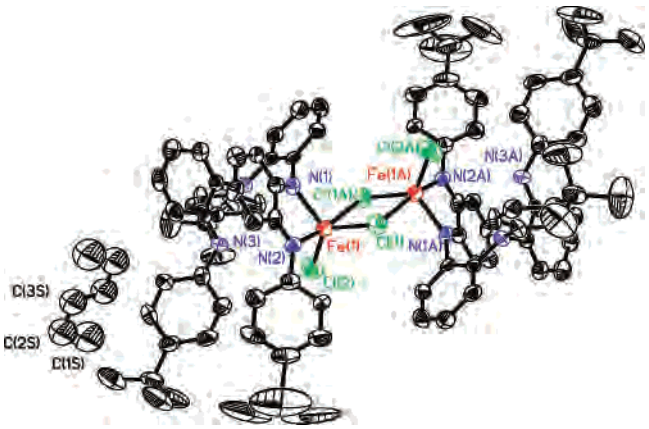

Figure 9. Solid-state structure of **9** showing 50% probability ellipsoids and the atom-labeling scheme. Selected interatomic distances (Å) and angles (deg): Fe(1)−N(1) 2.019(8), Fe(1)−N(2) 2.048(9), Fe(1)−Cl(2) 2.230(3), Fe(1)−Cl(1) 2.367(3), Fe(1)−Cl(1A) 2.515(3), Cl(1)−Fe(1A) 2.515(3), N(1)−C(1) 1.332(12), N(1)−C(45) 1.423(12), N(2)−C(2) 1.315(11), N(2)−C(3) 1.435(12), N(3)−C(18) 1.381(12), N(3)−C(13) 1.402(12), N(4)−C(24) 1.421(12), N(4)−C(40) 1.436(11), N(4)−C(23) 1.439(12); N(1)−Fe(1)−N(2) 78.8(3), N(1)−Fe(1)−Cl(2) 124.4(2), N(2)−Fe(1)−Cl(2) 102.0(2), N(1)−Fe(1)−Cl(1) 107.4(2), N(2)−Fe(1)−Cl(1) 89.2(2), Cl(2)−Fe(1)−Cl-(1) 128.08(13), N(1)−Fe(1)−Cl(1A) 192.6(3), N(2)−Fe(1)−Cl(1A) 167.6-(3), Cl(2)−Fe(1)−Cl(1A) 90.25(13), Cl(1)−Fe(1)−Cl(1A) 84.80(11), Fe-(1)−Cl(1)−Fe(1A) 95.20(11).

(2) Å] is consistent with the lower oxidation state of iron in compound **7**.

(b) Oxidation with $FeCl_3$. The oxidizing role of $Fe^{III}Cl$ moieties was further examined by dissolving equivalent amounts of **5** and anhydrous $FeCl_3$ in THF to obtain brown solutions of $[(L^1_{re-2}H)(Cl)Fe^{II}(\mu\text{-}Cl)_2Fe^{II}(Cl)(L^1_{re-2}H)]$ (**9**) as diamond-shaped crystals after extraction and crystallization from hexane.

The structure of **9** (Figure 9) reveals the presence of a centrosymmetric $[Fe^{II}(Cl)(\mu\text{-}Cl)]_2$ core, which is a well-established structural feature of many ferrous chloro-containing compounds.[25] Close inspection of the coordinated ligands indicates that each ligand is not only rearranged as demonstrated previously but also *doubly* oxidized within the vulnerable *o*-phenylenediamine moiety to afford a diamagnetic *o*-diiminobisquinone fragment (*o*-dibq^0; see below). Furthermore, only two amido (in effect, imino) residues are coordinated, whereas the third one is found to be at a nonbonding distance, presumably present as a protonated moiety. The doubly oxidized and singly protonated ligand ($L^1_{re-2}H$) in **9** is thus a monoanion. Although the reaction is certainly complicated, the reduction of the ferric sites and the oxidation of the ligand can be formally explained by means of a one-electron oxidation of **5** by $FeCl_3$ [thus reducing the latter to iron(II)], which, in combination with a second electron abstracted from the ligand by the iron(III) site of **5** (or a derivative thereof), results in a two-electron oxidative rearrangement of the ligand and reduction of the ferric site of **5**. This two-electron process is facilitated by the presence of chloride ligands in abundance, thus stabilizing the $[Fe^{II}(Cl)(\mu\text{-}Cl)]_2$ core.

Compound **9** possesses a crystallographic 2-fold axis penetrating the two bridging chloride atoms. The geometry around each five-coordinate iron atom is distorted trigonal bipyramidal. The equatorial coordination plane is defined by an imino nitrogen atom, the terminal chloride atom, and one bridging chloride atom (short $Fe-Cl_b$ bond), whereas the axial coordination is occupied by the second imino nitrogen atom and the second bridging chloride atom (long $Fe-Cl_b$ bond). Thus, each asymmetrically bridging chloride atom lies on the equatorial plane with respect to the proximal iron site and on the axis of the distal iron coordination. The other two nitrogen atoms reside beyond the coordination sphere of the iron center [Fe−N(3) = 3.981 Å; Fe−N(4) = 3.861 Å]. The N(3) atom is one of the amido nitrogen atoms of the original tripodal ligand (C−N bond distances are consistent with single-bond character) and is expected to be protonated. The N(4) atom is a bona fide three-coordinate amine residue. The $Fe-Cl_t$ bond distance [2.230(3) Å], the short and long $Fe-Cl_b$ bond distances [2.367(3) and 2.515-(3) Å], the $Cl_b-Fe-Cl_b$ bond angle [84.80(11)°], and the intermetallic Fe−Fe distance (3.607 Å) are all typical of the $[Fe^{II}(Cl)(\mu\text{-}Cl)]_2$ core unit, as established by similar ferrous chloro complexes carrying neutral bidentate ligands (for instance, $[(tmen)(Cl)Fe^{II}(\mu\text{-}Cl)_2Fe^{II}(Cl)(tmen)]$, where tmen = tetramethylethylenediamine).[25b]

Figure 10 depicts in greater detail the $[Fe^{II}(Cl)(\mu\text{-}Cl)]_2$ core and the coordinated *o*-dibq^0 moiety. Although the quality of the structural data is not optimal, metrical parameters strongly suggest that the two C−N bond distances represent double bonds [N(1)−C(1) 1.315(11) Å; N(2)−C(2) 1.332(12) Å] and the phenylene ring is characterized by the usual pattern of four long [C(1)−C(2) 1.464(14) Å; C(2)−C(10) 1.448-

(25) (a) Raper, E. S.; Miller, A.; Glowiak, T.; Kubiak, M. *Trans. Met. Chem.* **1989**, *14*, 319−320. (b) Cotton, F. A.; Daniels, L. M.; Murillo, C. A. *Inorg. Chim. Acta* **1994**, *224*, 5−9. (c) Mills, D. K.; Hsiao, Y. M.; Farmer, P. J.; Atnip, E. V.; Reibenspies, J. H.; Darensbourg, M. Y. *J. Am. Chem. Soc.* **1991**, *113*, 1421−1423.

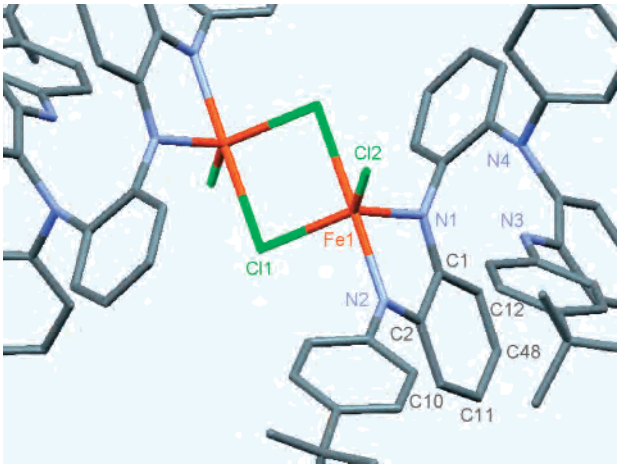

Figure 10. Close-up picture of the *o*-dibq^0 moiety in **9**.

(13) Å; C(11)−C(48) 1.412(14) Å; C(12)−C(1) 1.434(14) Å] and two short [C(10−C(11) 1.336(13) Å; C(12)−C(48) 1.361(13) Å] C−C bond distances. Similar metrical parameters are found in many other *o*-dibq^0-containing compounds, ([Fe^{II}(dibq)$_3$]$^{2-}$,[26] [Fe^{II}(CN)$_4$(dibq)$_3$]$^{2-}$,[27] and [Os^{II}(dibq)$_3$]$^{2-}$.[28] The presence of two diamagnetic *o*-dibq^0 moieties and a diferrous site is also consistent with the EPR-silent (X-band) character of **9**.

Conclusion

The following is a summary of the principal findings of this investigation:

(1) A new family of tripodal trisamidoamine ligands has been introduced that is capable of providing significant electron density and steric protection to a coordinated metal center but could also store oxidizing equivalents under specific conditions.

(2) A series of electron-rich [(L^1)Fe^{II}solv]$^-$ compounds (solv = DMF, CH_3CN) have been isolated or generated in situ, which are exceedingly air-sensitive and can be transformed to a series of [(L^1)Fe^{III}OH]$^-$ compounds featuring terminal hydroxo groups.

(3) The [(L^1)Fe^{II}solv]$^-$ series of compounds can reductively dechlorinate organochlorides (R−Cl reactivity order R = benzyl, allyl > *t*-Bu, *i*-Pr ≫ *n*-Bu, Ph) and generate the synthetically useful [(L^1)Fe^{III}solv] species. The latter can be oxidized by the strong oxidant $FeCl_3$ to effect complete reduction of all iron to iron(II) (captured in a [Fe^{II}(Cl)(μ-Cl)]$_2$ core) along with oxidative rearrangement of the ligand featuring doubly oxidized *o*-diimidophenylene rings.

(4) Efforts to synthesize [(L^1)Fe−O−Fe(L^1)]$^{2-}$ via the [Cl_3Fe−O−$FeCl_3$]$^{2-}$ precursor indicate that intrinsic Fe^{III}Cl moieties can perform ligand oxidation, resulting in a species ([(L^1_{re})(Cl)Fe^{II}]$^{2-}$) in which all iron has been reduced and the ligand has been oxidatively rearranged, although the oxidation equivalent has not been retained. This compound can be easily oxidized to [(L^1_{re})(Cl)Fe^{III}]$^-$ by dichloromethane.

Future studies will be directed toward exploring whether these and related ligand systems can store oxidizing equivalents above the L$^{\bullet}Fe^{III}$ level in accordance with chemistry encountered with P450 oxygenases,[29] peroxidases,[30] and related synthetic analogues.[31]

Acknowledgment. We thank Dr. Charles Barnes for assistance with X-ray analysis results. We are indebted to Dr. Nicholas Leventis for insightful comments. We gratefully acknowledge generous financial support (to P.S.) by the NSF (Grant CHE-0412959) and, in part, by the NIH/NIEHS (Grant 5 P42 ES007381). We also acknowledge NSF funding (Grant CHE-0420497) for the purchase of the diffractometer at the University of Missouri—St. Louis.

Note Added in Proof: While this work was under review, a high-yield synthesis of the precursor 2,2′,2″-triaminotriphenylamine appeared in the literature.[32] This precursor has been previously reported in the Ph.D. thesis of Dr. R. Çelenligil-Çetin.[33]

Supporting Information Available: Listings of experimental procedures, solid-state structures of 2,2′,2″-triaminotriphenylamine (Figure S1), ligand L^1H_3 (Figure S2), and compound **3** (Figure S3), X-ray crystallographic tables for 2,2′,2″-triaminotriphenylamine, L^1H_3, and compounds **1**−**9** (Tables S1−S66), and X-ray crystallographic data for the same compounds in CIF format. The material is available free of charge via the Internet at http://pubs.acs.org.

IC702154Z

(26) Peng, S.-M.; Chen, C.-T.; Liaw, D.-S.; Chen, C.-I. *Inorg. Chim. Acta* **1985**, *101*, L31−L33.
(27) Christoph, G. G.; Goedken, V. L. *J. Am. Chem. Soc.* **1973**, *95*, 3869−3874.
(28) Ghosh, A. K.; Peng, S.-M.; Paul, R. L.; Ward, M. D.; Goswami, S. *J. Chem. Soc., Dalton Trans.* **2001**, 336−340.
(29) Groves, J. T. *J. Inorg. Biochem.* **2006**, *100*, 434−447.
(30) Derat, E.; Shaik, S. *J. Am. Chem. Soc.* **2006**, *128*, 13940−13949.
(31) Balch, A. L.; Chan, Y.-W.; Cheng, R.-J.; La Mar, G. N.; Latos-Grazynski, L.; Renner, M. W. *J. Am. Chem. Soc.* **1984**, *106*, 7779−7785.
(32) Jones, M. B.; MacBeth, C. E. *Inorg. Chem.* **2007**, *46*, 8117−8119.
(33) Çelenligil-Çetin, R. Synthesis, Characterization, and Reactivity of Iron Complexes with N-Donor Ligands in Relation to Oxygenation of Hydrocarbons. Ph.D. Thesis, Boston University, Boston, MA, 2004.